Landslide Hazard Zonation Mapping Using Binary Logistic Regression and its Validation in Mandakini Valley, Garhwal Himalaya

Suman Das[1] and Ashish Kumar Saha[2]

Abstract

Landslides frequently occur in mountainous regions globally, posing risks to human settlements, lives, livelihoods, and infrastructure. The monsoon season in June 2013 began two weeks ahead of its typical schedule in Uttarakhand. Between June 15 and June 17, 2013, intense rainfall and cloud bursts affected numerous areas in the upper Himalayan region. Landslides are complex phenomena that are influenced by a variety of factors, including rock composition, strength of the rock mass, and other physical characteristics. In the Himalayan region, landslides occur in different types and dimensions and have generic variations. The present study focused on Landslide Hazard Zonation (LHZ) in the Mandakini watershed, which is part of the Garhwal Himalaya region. The dataset for this study comprises 18 landslide conditioning factors along with the landslide inventory map of the region. Training data (70%) and testing data (30%) were then separated from the landslide inventory data. The Binary Logistic Regression (BLR) of Maximum likelihood estimation is used with the logit variable (derived from the dependent variable) to assess the probability of landslides in the area. The model was validated based on the ROC curve. It was observed that the binary logistic regression model selected 82 out of 102 initial independent variables. The BLR model attained a prediction accuracy of 89.6%, effectively classifying binary training data. In the accuracy assessment through ROC, 91.4% were achieved using testing data. The LHZ map provide valuable insight to understand the landslide hazard in the Mandakini valley especially after 2013 Kedarnath disaster. The research will further help in effective planning and landslide mitigation strategies for comprehensive landslide disaster management over the study area.

Keywords: *Landslide, LHZ, BLR, ROC, Mandakini Valley, Himalaya*

[1] Department of Geography, Kirori Mal College, University of Delhi, Delhi – 110007
[2] Department of Geography, Delhi School of Economics, University of Delhi, Delhi – 110007

1. Introduction

Landslides frequently occur in mountainous regions globally, posing risks to human settlements, lives, livelihoods, and infrastructure. The monsoon season in June 2013 began two weeks ahead of its typical schedule in Uttarakhand. Between June 15 and June 17, 2013, intense rainfall and cloud bursts affected numerous areas in the upper Himalayan region. Landslides are intricate phenomena influenced by various factors, including rock composition, strength of the rock mass, and other physical characteristics. In the Himalayan region, landslides occur in different types and dimensions and have generic variations. The present study focused on Landslide Hazard Zonation (LHZ) in the Mandakini watershed. The Himalaya are vulnerable to numerous natural hazards owing to their geo-dynamically active characteristics and distinct weather patterns. An initiative for mapping landslide hazards would aim to pinpoint regions susceptible to landslides based on geological and topographical factors as well as the current landslide situation (Mathew et al., 2007). The likelihood of landslide hazards, which is characterized as the chance of potentially destructive events occurring in a specific location, depends on various environmental factors that influence this risk. A landslide hazard zonation (LHZ) map offers advanced insight into potential landslide zones based on a set of geo-environmental elements conducive to landslides. It also helps in implementing mitigation techniques following any landslide threat. The premise of LHZ relies on the belief that future landslides are likely to occur in areas that share similar geo-environmental conditions to those found at present and historical landslide sites. (van Beek, 2002; Kanungo et al., 2012). Landslide Hazard zonation,' (LHZ) refers to the likelihood of landslide occurrences within a geographical area, determined by various geo-environmental factors. (Kayastha et al., 2013 Kundu et al., 2013; Bisht et al., 2018). The primary objective of landslide hazard mapping is to reduce the losses of human life and economic assets. A landslide hazard map provides crucial information about locations where landslides may happen in the future by highlighting regions with previous landslide events and areas that share similar physical features (van Westen et al., 2006). A landslide hazard zonation (LHZ) map can significantly mitigate the risk associated with possible landslides through the implementation of suitable management strategies and in the course of planning forthcoming

development projects. The dependability of these landslide hazard maps is influenced by the data quality and the methods or models employed in their creation (Ayalew and Yamagishi, 2005).

The selection of factors that influence landslides relies on the availability of data, the expertise of professionals, and comprehensive field investigations. The advantage of the machine learning technique is that it is a fast computation package, easy data availability, and Geographical Information systems (GIS) have given new thrust into landslide hazard research (Hadmoko et al., 2010; Pradhan & Lee, 2010; Tien Bui et al., 2012; Li et al., 2013; Qiu et al., 2017). The precision of a hazard map relies significantly on the effective integration of environmental elements that lead to landslides. Consequently, it is essential to comprehend how each factor contributes to landslide events and to examine the relationships between these factors in order to assess the likelihood of landslides occurring in a specific region.

Numerous approaches and techniques have been suggested to evaluate landslide hazards. Regardless of the variations, all the methods and processes rely on a limited number of assumptions (Pardeshi et al., 2013). First, landslides leave sensible signs, such signs can be recognized, categorized, and mapped through the analysis of satellite imagery or in the field (Mondini et al., 2011; Thanh and De, 2012; Guzzetti et al., 2012). Second, landslides and their circumstances are governed by physical properties that can be examined empirically, deterministically or statistically. Conditions that activate landslides, directly or indirectly related to slope failures, can be used to frame predictive models for the spatial occurrence of landslides (Dietrich et al., 1995). Third, for landslide studies, "the past and present are keys to the future" (Carrara & Guzzetti, 1995). This assumption indicate that future landslides are more probable under analogous conditions, so facilitating an understanding of both history and present instability (Furlani & Ninfo, 2015). Lastly, the spatial occurrence of landslides can be analyzed through heuristic investigation, calculated through physical models or through the analysis of environmental information. Hence, a territory can be classified based on various susceptibility classes ranked based on different probabilities (Carrara et al.,

1995; Glade & Crozier, 1996). Approaches and techniques for assigning landslide hazards can be qualitative or quantitative. Qualitative methods are inherently subjective, evaluate vulnerability through heuristic techniques, and express risk levels with descriptive language. In contrast, quantitative approaches yield numerical estimates, or in other terms, probabilities related to landslide occurrences within specific hazard zones (Guzzetti et al., 1999).

Quantitative methods in Statistical approaches analyze the functional relationships between known factors of slope instability and the distribution of landslides, both historical and current (Huabin et al., 2005; Van Westen et al., 2008). An examination of the literature database indicates that methods grounded in statistics and those based on physical principles are favoured for determining landslide susceptibility in quantitative terms. Reichenbach et al. (2014) examine statistically-based modelling methods and terrain zonation. They use the words "susceptibility modeling" and "modeling" to refer to landslide susceptibility modelling. With the development of geospatial technologies and improved computational resources, research on landslides has evolved significantly. The integration of GIS and remote sensing has demonstrated its effectiveness as a valuable tool for conducting landslide hazard assessments (van Westen et al., 2003). The Geographical Information System (GIS) has played a role in structuring the database and performing mathematical modelling. Over the past forty years, researchers worldwide have conducted numerous studies on landslide hazard assessment utilizing both quantitative and qualitative models enhanced by remote sensing and GIS methodologies. (Pradhan and Lee, 2010; Tien Bui et al., 2011; Li et al., 2013; Qiu et al., 2017). The thematic layers related to the causes of landslide events have been developed using remote sensing techniques, along with ancillary data.

2. Study Area

The present study focused on the Mandakini watershed (Figure 1), which is fall in Rudraprayag district of Uttarakhand. Mandakini valley spans approximately 1,646 sq. kms. It consists of the Lesser and Higher Himalayan terrain of Garhwal Himalaya. Mandakini watershed stretches from Kedarnath in the north to Rudraprayag in the south, situated between 30°15'N to 30°45'N and 78°45'E to 79°30'E. It falls within Survey of India Toposheet numbers - 53J /14, 53J/15, 53N/1, 53N/2, 53N/3, 53N/4, and 53N/6.

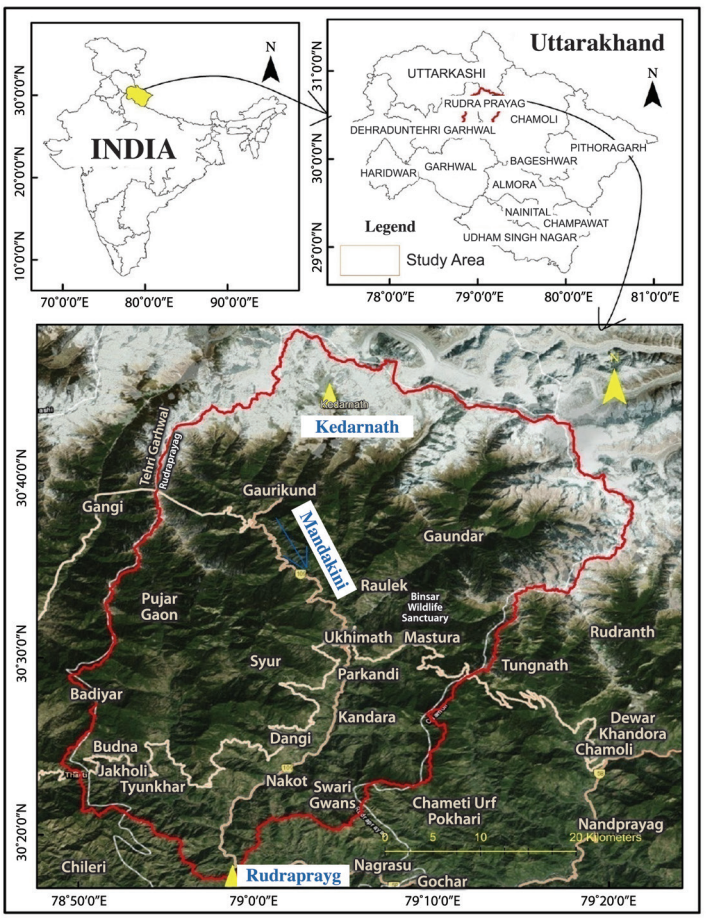

Figure 1 : Study area, Mandakini Valley

Source : Das & Saha., 2020.

Rudraprayag town is located at the confluence of Mandakini and Alaknanda rivers. The Mandakini River traverses the Main Central Thrust (MCT), which delineates the boundary between the Higher Himalaya and the Lesser Himalaya. The MCT zone is characterized by numerous faults and consists of fractured and weathered rock formations. The primary roadway within this watershed provides connectivity from Sonprayag in the north to Rudraprayag in the south. Beyond Sonprayag, individuals undertake a trek of approximately 17 kilometres to reach Kedarnath town, renowned

for its historical and cultural significance, as it is home to the esteemed Kedarnath Temple (Naithani et al., 2011; Sati et al., 2011; Sati & Gahalaut, 2013). The catchment exhibits a diverse array of rock types, with geological ages spanning from the Palaeoproterozoic to the Mesoproterozoic period. The rock succession exposed in the study area is categorised into two groups, the rock sequences between Main Central Thrust (MCT) and Main Boundary Fault (MBF), which constitute the Lesser Himalaya, and the rock sequences located north of Main Central Thrust (MCT), which comprise the Higher Himalaya.

3. Materials and Methods

To create a landslide susceptibility map, it is crucial to develop a spatial database that includes several factors related to landslides. Data from satellite sensor IRS-1D LISS IV multispectral digital data with spatial resolution of 5m and IRS Cartosat-1 Pandigital stereo data with spatial resolution of 2.5m were used for this study. The topographic parameters including lope, slope length, elevation, curvature and convergence index, were from Cartosat DEM, while environmental factors, including Normalised Difference Vegetation Index (NDVI), and land use land cover (LULC) extracted through LISS IV multispectral digital data. The spatial data pertinent to landslide hazard zonation can be divided into three principal categories: landslide inventory data, environmental factors, and triggering factors (van Westen et al., 2006).

3.1. Landslide Inventory

The landslide inventory map is the backbone of the landslide study. The initial critical step in conducting landslide hazard assessments involves gathering data on prior landslide events. This information is essential for informing and improving future spatial predictions (Ercanoglu & Gokceoglu, 2004). In this study, an image interpretation technique was used to obtain a multi-temporal landslide inventory map. Landslides exhibit distinctive characteristics in remote sensing images and aerial photographs, including aspects like colour, shape, shadow, and variations compared to the surrounding terrain (Yang et al., 2010; Guzzetti et al., 2012; Sun et al., 2018). High-resolution Google Earth data of the Kedarnath disaster time, along with SRTM DEM data, were used as the primary data product for generating the multi-temporal

landslide inventory. The following steps were used to map a landslide polygon in ArcGIS and build its inventory attribute. In total, 5.30 sq. km. of landslides were identified in the post-disaster landslide inventory (Figure 2b) and mapped from the digitally enhanced Google Earth satellite images based on the tone, texture, and size of the landslide (Figure 2a). The landslides were field-checked along NH 109, Kalimath Road, Okhimath Road, and the foot track to Kedarnath.

Most of the landslides occur within a distance of less than 30 m on either side of the road and might have resulted from the removal of the toe or the cutting of roads. Riverbank failures due to toe erosion by drainages/nalas are also common in the study area, especially along the Mandakini River and its tributaries passing through the area. Most of the landslides are shallow translational debris/rock slides, with a depth of slip plane being less than 5 m. The landslide inventory has been separated into training and testing/validation datasets, with 70% assgned for training and 30% allocated for testing and validation. This division was conducted through random splitting, as the temporal data regarding landslide occurrences was not available.

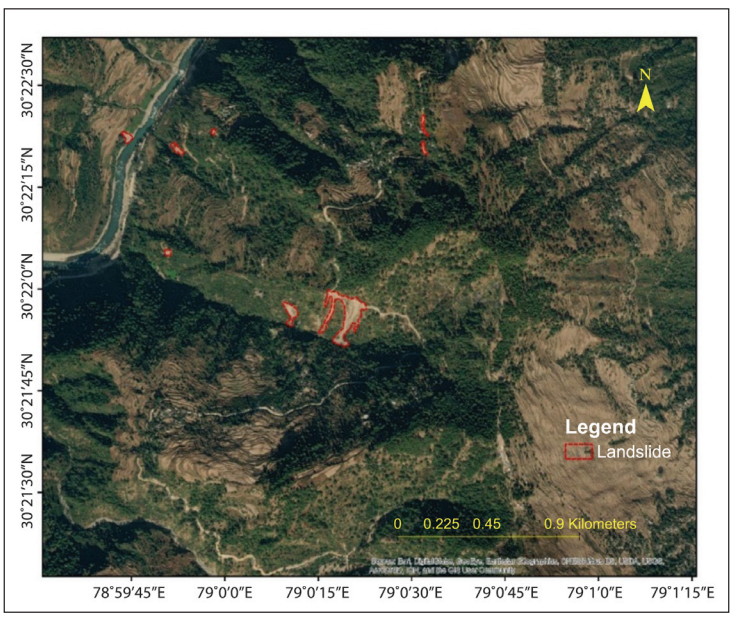

(a)

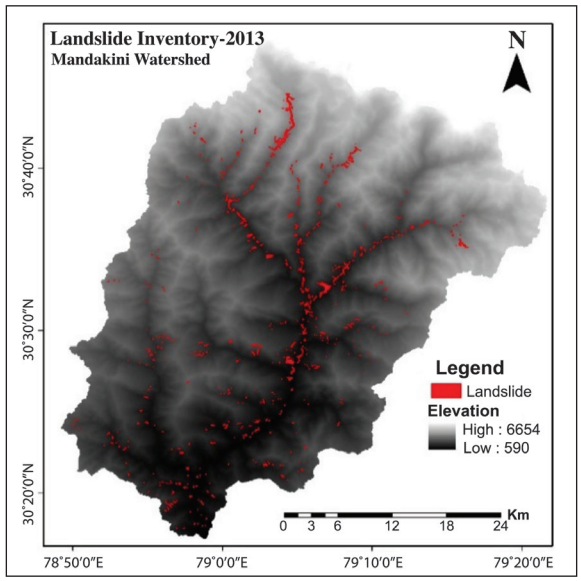

(b)

Figure 2 : Landslide Inventory using Google Earth Image (a) & Landslide Inventory Map of the Study Area (b).

3.2. Elevation

While elevation does not directly cause landslides, it interacts with various other factors such as tectonic activities, weathering processes, erosion and precipitation. Consequently, elevation plays a significant role in landslide occurrence and affects the overall system (Rozos et al., 2011). The elevation map was generated using the CARTOSAT DEM in Arc GIS software. The classification of the DEM was done using natural break methods (Li et al., 2013; Arabameri et al., 2020). The elevation varies from 590 m to 6654 m in the study area (Figure 2b). For the present study, the elevation was subdivided into five classes: < 1725 m, 1725–2511 m, 2511–3400 m, 3400–4404 m, and > 4404 m, respectively (Figure. 3a).

3.3. Slope

The degree of slope is a significant factor that impacts slope stability (Pourghasemiet al., 2012b; Lee & Min, 2001). This conditioning factor is commonly utilized in the

preparation of landslide hazard maps (Pourghasemi et al., 2012a & b). The slope for the present study area was derived from the digital elevation model (DEM) and classified into five distinct categories using the natural break method (Figure 3b), i.e., <15.71°, 15.71° - 25.03°, 25.03° - 33.47°, 33.47° - 42.78° and > 42.78°. In the slope angle, the highest area covered by class three covers 28.80% of the total geographical area, followed by class two, four one, and five, which cover an area of 26.08%, 21.70%, 19.99%, and 9.43%, respectively.

3.4. Slope Aspect

The slope aspect has been identified as a significant contributing factor to the occurrence of landslides (Lee et al., 2004; Pourghasemi et al., 2012a). The characteristics of slope aspect within the study area were obtained using the Digital Elevation Model (DEM)., using Arc GIS, and it was categorized into nine classes; i.e., north, northeast, east, southeast, south, southwest, west, northwest and flat, to illustrate the corelations between aspect and landslides (Figure 3c).

3.5. Curvature

The curvature funcation as a marker of the erosional susceptibility of the slopes as well as the existing slope morphology (Sharma & Mahajan, 2018). In this study, a plan curvature map was generated using ArcGIS GIS software and classified into three categories: concave, planar, and convex. This classification was based on specific criteria: a profile curvature of less than -0.1 indicates convex slope morphology; a profile curvature between -0.1 and 0.1 denotes linear slope morphology; and a profile curvature greater than 0.1 signifies concave slope morphology (Zhang et al., 2012), which are illustrated in the accompanying curvature thematic map (Figure 3d).

3.6. Slope Length

Slope length is considered one of the topographical factors that influence the occurrence of landslides. Many researchers (i.e., van der Knijff et al., 2000; Kumar & Anbalagan, 2015; Arabameri et al., 2020) consider slope length as a landslide

conditioning factor in their studies. The slope length of the terrain is classified into five different classes, i.e., < 14.82 m, which cover an area of 72.95%, 14.82 m – 45.82 m, 45.82 m – 83.57 m, 83.57 m – 133.44 m and > 133.44 m (Figure 3e).

3.7. Relative Relief

Relative relief refers to the variation between the minimum and maximum altitudes within a defined area or facet, and it is determined through spatial analysis (Pandey et al., 2008). The relative relief is calculated in the Arc-GIS environment using the DEM data. The range of relative relief (Figure. 3f) was found to be 915.83–3117.21 m. Further, it is classified into five classes, i.e., < 1433.80 m, 1433.80-1684.15 m, 1684.15-1977.67 m, 1977.67-2374.78 m, and >2374.78 m.

3.8. Convergence index (CI)

The convergence index is a critical topographic factor that significantly influences landslide occurrences within a particular region. The convergence index (CI) provides a metric for assessing whether flow within a cell diverges (convergence index < 0) or converges (convergence index > 0), (Claps et al., 1996). CI map prepared using a tool in SAGA-GIS (Figure. 4a).

$$CI = \left(\frac{1}{8} \sum_{i=1}^{8} \theta_i \right) - 90^{\circ} \qquad \text{Eq. 1}$$

Where θ denotes the mean angle created between the aspects of neighboring cells and the orientation towards the central cell.

3.9. Lithology

Distinct lithological units exhibit varying landslide hazard values, making them a critical component in landslide hazard assessments (Pourghasemi *et al.*, 2012b; Yalcin & Bulut, 2007). The lithological mapping of the region (Figure. 4b) indicates the presence of the Vaikrita Formation in the northern area, characterized primarily by coarse mica-garnet-kyanite and sillimanite-bearing psammitic metamorphics. This formation constitutes a

significant portion of the Greater/Higher Himalaya in Garhwal. These rocks contribute to a highly rugged topography, featuring deep gorges and high peaks, with the higher altitudes predominantly snow-covered, resulting in the formation of U-shaped broad valleys characteristic of a glacial landscape. This geological group is intruded by Tertiary pegmatites and granites, specifically the Badrinath Granite, which facilitates the development of migmatites, biotite-rich schists, and calc-schists. The mineral assemblages observed suggest a medium to high-grade metamorphism, comparable to the amphibolite facies found in the rocks of the Vaikrita Group (Valdiya, 1980). The Munsiari Formation, located to the south of this geological feature, is found within the Lesser Himalaya. This formation comprises a range of rock types, including meso- to epi-grade para- and ortho-gneisses, schists, calc-silicate rocks, marbles, granites, and their corresponding mylonitic equivalents (Choubey *et al.*, 1999). South of the Munsiari Formation, the Ramgarh Group is Present. The primary rock formations consist of dark green chloritic and greenish-brown schist, finely layered biotite-rich coarse-grained schist, interbedded sericite-chlorite-quartz schist, and porphyroid (Chahal *et al.*, 2017). The high landslide hazard in the Mandakini watershed is due to complicated geological settings, changing slopes and relief, substantial rainfall, and ever-increasing human intervention in the ecosystem (Kumar & Anbalagan, 2019). Extreme climatic events contribute to the instability of the terrain, as exemplified by the Kedarnath disaster (Dubey *et al.*, 2013).

3.10. Thrust

A map illustrating the significant thrusts traversing the study area (Figure 2.1) has been prepared upon the work of Valdiya (1980) and Khanduri *et al.* (2018). The Main Central Thrust (MCT) represents the primary geological feature, forming an extensive area between Rambara and Kund (Valdiya, 2014; Sundriyal et al., 2015) characterized by rocks that have been significantly sheared, fractured, and crushed due to tectonic processes (Chahal *et al.*, 2017). Apart from the MCT, VT and Banswara Thrust are the significant structures found in the study area. The following buffer zones were designated around these thrusts: < 500, 500–1000, 1000–1500, 1500-2000, and >2000 m. in Arc-GIS (Figure. 4c) using the Euclidean distance tool. The presence of the Main Central Thrust zone contributes to significant shearing and fracturing within the region, resulting in rock instability and an increased susceptibility to landslides and other natural hazards.

3.11. Distance from Faults

Faults represent a weak line or zone distinguished by intensely fractured geological formations (Fell *et al.*, 2000). Alaknanda Fault, Mandakini Fault, Rawan Ganga Fault, Madhyamaheshwar Fault, Laster fault and Kyunja Fault are among the tectonic interactions found in the region. These significant faults are aligned along the main channel course of the valleys. The distance from faults was divided into five categories with an interval of 500 m (Sahana and Sajjad., 2017) in Arc-GIS using the Euclidean distance tool (Figure. 4d).

3.12. Lineament

The study area's photo-lineament (buffer) map was extracted from the LISS - IV satellite image as polyline features. A lineament is a linear feature of the surface, whether simple or composite, that can be mapped and has components that are aligned either straight or slightly curved. These features are distinctly different from the pattern of surrounding elements and indicate a subsurface phenomenon (van & Seijmonsbergen, 2006; Hamza & Raghuvanshi, 2017). Near the lineaments, the likelihood of landslide occurrences is deemed greater compared to regions located farther from the lineaments. The distance to lineament was calculated using the Euclidean distance tool with an interval of 500 m in Arc-GIS and categorized into five buffer zones of < 500, 500–1000, 1000–1500, 1500-2000, and >2000 m (Figure. 4e).

3.13. Distance to Drainage

Drainage networks have the potential to negatively impact slope stability through mechanisms such as toe undercutting or by saturating the material that forms the slope. Consequently, the distance to drainage layers has been analyzed using GIS (Saha et al., 2005). Based on the extracted drainage, a map of proximity to the drainage network was generated using the Arc-GIS Euclidean distance tool (Arabameri et al., 2020). In this study, five distinct buffer zones were produced in the study area, e.g., 0–100, 100–200, 200–300, 300-400, and more than 500 m (Figure 4f).

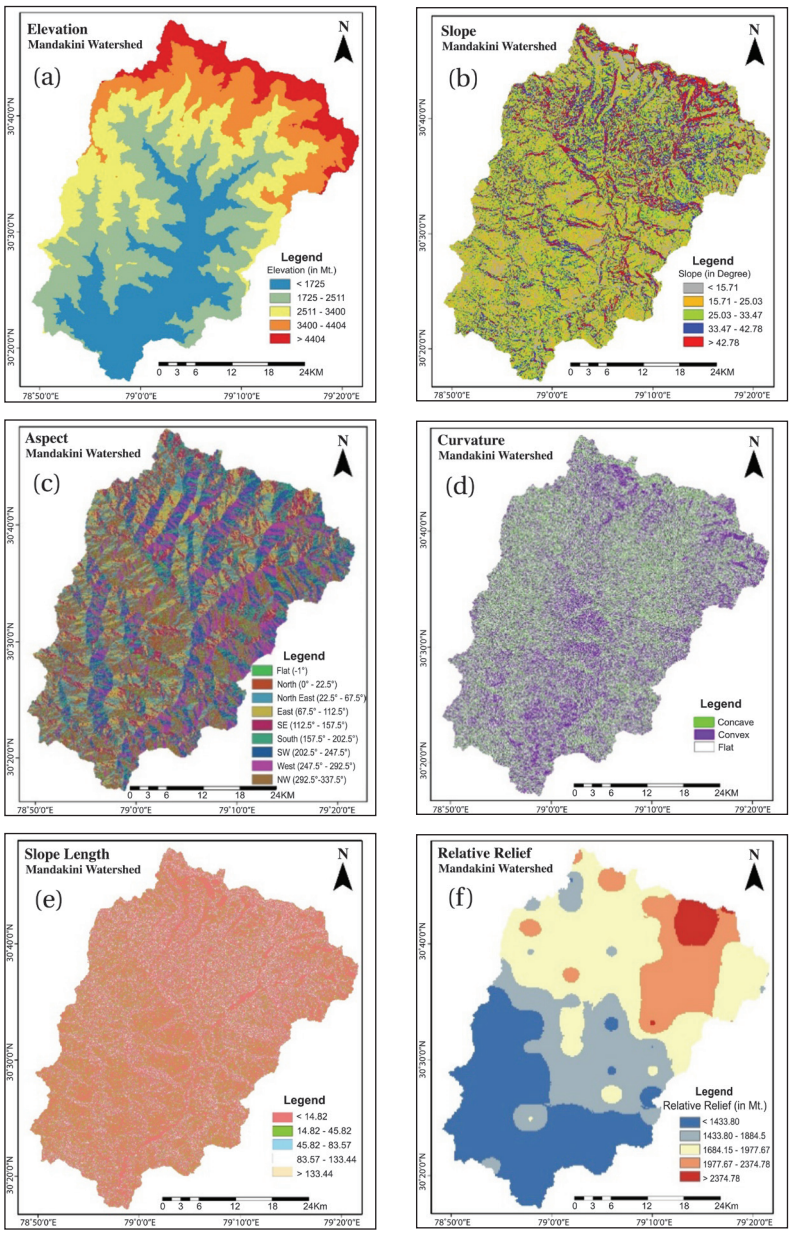

Figure 3 : Landslide Causative Factors – Elevation (a), Slope (b), Aspect (c), Curvature (d), Slope Length (e) & Relative Relief (f).

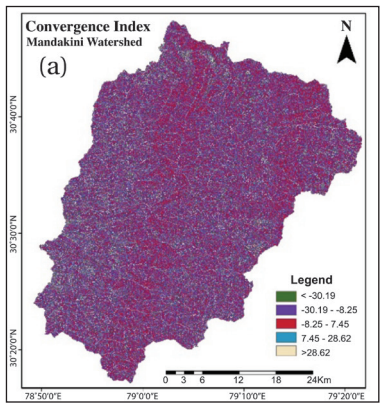
Convergence Index
Mandakini Watershed
(a)
N
Legend
< -30.19
-30.19 - -8.25
-8.25 - 7.45
7.45 - 28.62
>28.62
0 3 6 12 18 24Km
30°40'0"N
30°30'0"N
30°20'0"N
78°50'0"E
79°0'0"E
79°10'0"E
79°20'0"E

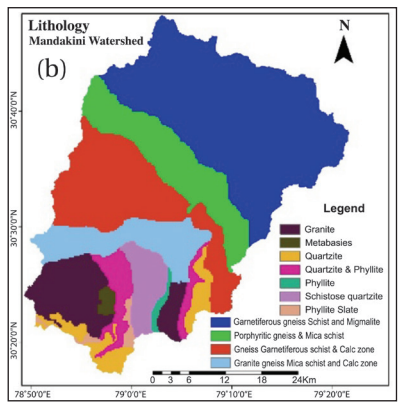
Lithology
Mandakini Watershed
(b)
N
Legend
Granite
Metabasies
Quartzite
Quartzite & Phyllite
Phyllite
Schistose quartzite
Phyllite Slate
Garnetiferous gneiss Schist and Migmalite
Porphyritic gneiss & Mica schist
Gneiss Garnetiferous schist & Calc zone
Granite gneiss Mica schist and Calc zone
0 3 6 12 18 24Km
30°40'0"N
30°30'0"N
30°20'0"N
78°50'0"E
79°0'0"E
79°10'0"E
79°20'0"E

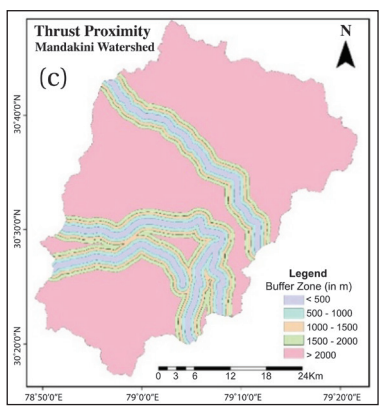
Thrust Proximity
Mandakini Watershed
(c)
N
Legend
Buffer Zone (in m)
< 500
500 - 1000
1000 - 1500
1500 - 2000
> 2000
0 3 6 12 18 24Km
30°40'0"N
30°30'0"N
30°20'0"N
78°50'0"E
79°0'0"E
79°10'0"E
79°20'0"E

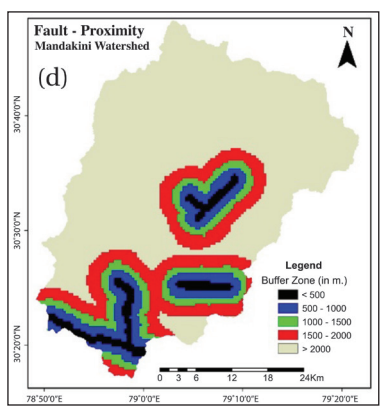
Fault - Proximity
Mandakini Watershed
(d)
N
Legend
Buffer Zone (in m.)
< 500
500 - 1000
1000 - 1500
1500 - 2000
> 2000
0 3 6 12 18 24Km
30°40'0"N
30°30'0"N
30°20'0"N
78°50'0"E
79°0'0"E
79°10'0"E
79°20'0"E

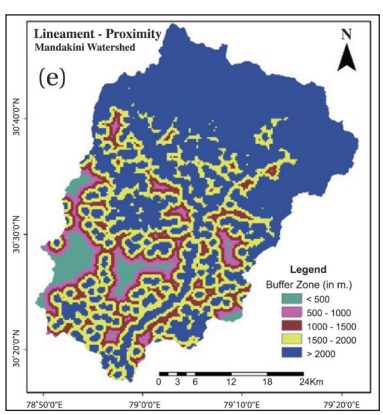
Lineament - Proximity
Mandakini Watershed
(e)
N
Legend
Buffer Zone (in m.)
< 500
500 - 1000
1000 - 1500
1500 - 2000
> 2000
0 3 6 12 18 24Km
30°40'0"N
30°30'0"N
30°20'0"N
78°50'0"E
79°0'0"E
79°10'0"E
79°20'0"E

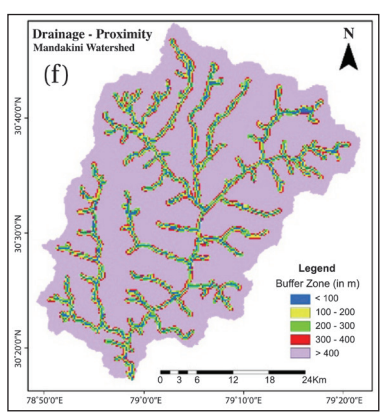
Drainage - Proximity
Mandakini Watershed
(f)
N
Legend
Buffer Zone (in m)
< 100
100 - 200
200 - 300
300 - 400
> 400
0 3 6 12 18 24Km
30°40'0"N
30°30'0"N
30°20'0"N
78°50'0"E
79°0'0"E
79°10'0"E
79°20'0"E

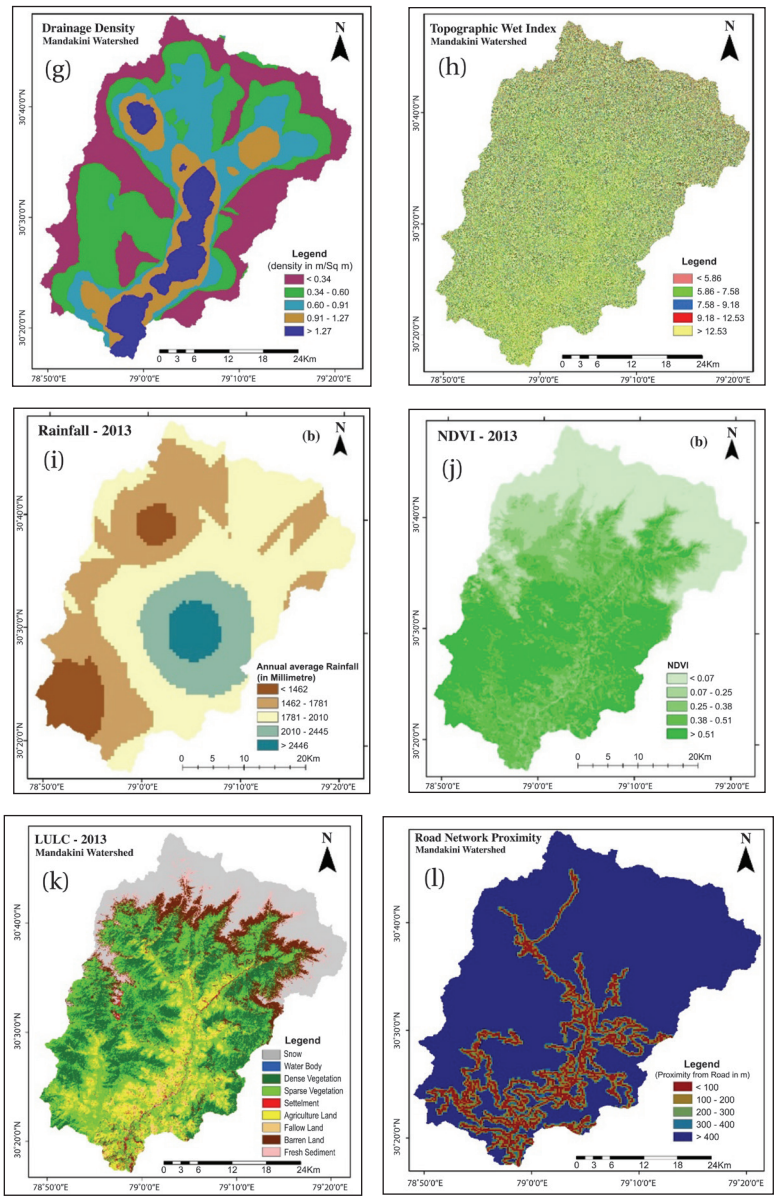

Figure 4 : Landslide Causative Factors – Convergence Index (a), Lithology (b), Thrust (c), Fault (d), Lineament (e) Drainage (f), drainage Density (g), TWI (h), Rainfall (i), NDVI (j), LULC (k) & Road Network (l).

3.14. Drainage Density

The total length of drainage channels within a unit area of a river basin is known as the Drainage Density (Horton, 1945). The study by Dahal et al. (2008b) shows that the areas with higher drainage density are typically more vulnerable to shallow-seated landslides during heavy rainfall, whereas the large-scale landslide is frequent in areas with lesser drainage density. Drainage density was calculated using line density tools in Arc GIS (Saha et al., 2002, 2005) and divided into five classes: 0–14.80, 14.80–40.29, 40.29–68.24, 68.24–108.53, and > 108.53m/sq m (Figure. 4g).

3.15. Topographical Wet Index (TWI)

It is another topographic factor within the runoff model (Pradhan and Kim, 2014; Wang et al., 2015). TWI is calculated as:

$$TWI = In\left(\frac{S}{\tan \alpha}\right) \quad \text{Eq. 2}$$

Where S denotes the specific catchment area for each cell, and β signifies the slope gradient (measured in degrees) of the topographical elevations (Moore *et al.*, 1991; Saadatkhah et al., 2015). In the present study, the TWI was calculated using the tool in SAGA-GIS, and values were arranged in five classes through the natural break method (NBM) of Jenk's in Arc GIS: 0 to 5.86, 5.86 – 7.58, 7.58–9.18, 9.18- 12.53 and > 12.53 as shown in the Figure 4h.

3.16. Rainfall

Rainfall is an important trigging factor in landslide occurrence in Himalaya from the beginning of June to the end of September; thus, it is another significant parameter in landslide hazard zonation. In this study, an annual rainfall map was generated by using the weather data of fifteen stations of the Indian Meteorological Department (IMD) in the area and its elevation of surrounding localities by applying the Co-kriging (Eq. 3) interpolation method (Goovaerts, 2000),

$$z^{*}_{CK}(u) = \sum_{a=1}^{n(u)} \lambda_{\alpha}^{CK}(u) Z(u_{\alpha}) + \lambda^{CK}(u)[y(u) - m_y + m_Z], \quad \text{Eq. 3}$$

The interpolation was done using Arc-GIS environment, classified into five classes through natural break method (NBM) of Jenk's in GIS (Figure. 4i), where the minimum rainfall was 1033 mm/year and maximum rain was 3217 mm/year in 2013.

3.17. Normalized Difference Vegetation Index (NDVI)

A high vegetation density can reduce the probability of landside occurrence and also defer soil transmission and erosion, while a high probability of landslide occurrence can be found in the low vegetation area (Arabameri et al., 2020). The NDVI values varied from -0.12 to +0.68 (Figure. 4j). The NDVI is further categorized into five sub-layers for using the natural break method.

3.18. Land Use and Land Cover (LULC)

The distribution of land cover plays a critical role in influencing slope conditions related to landslide occurrences (Lee et al.,2013). The present study used IRS-1D and LISS-IV remote sensing data to map land cover. In order to improve the result and achieve higher accuracy then using spectral data from a remote sensing sensor alone, the LISS-IV, multispectral image with spatial resolution of 5m was used as the primary data for creating the LULC map of the study area. Additionally, ancillary data, such as the DEM from Cartosat 1 and NDVI (Figure 4k) extracted from the LISS-IV image also incorporated into the sensing classification process in this study. In this study, the supervised classification of the Maximum Likelihood classifier (MLC) was used on the Erdas Imagine platform. The LULC is classified into nine categories, namely – Snow, Water Body, Dense Vegetation, Sparse Vegetation, Agricultural Land, Fallow Land, Barren Land, Fresh Sediment and Settlement (Figure 4k). Various LULC classes over the Mandakini watershed indicate the significant impact of 2013 Kedarnath disaster on LULC (Das & Saha., 2020). The study shows that dense and sparse vegetation classes cover 22.05% and 27.03%, respectively. At the same time, the agricultural land covers

an area of about 12.08% and fallow land of 3.22%. In the category of Barren, land and fresh sediment cover 9.17% and 3.95%, respectively.

3.19. Proximity to the Road

In, Himalaya most of the landslides were observed along the road. Distance from the road has been produced through proximity analysis. (Mathew et al., 2009). Using Google Earth Image and Survey of India toposheets as a reference map, a polyline feature of the NH-109, Kalimath-Okhimath road and other PWD roads were prepared. The distance to roads was determined using the Euclidean distance tool in the ArcGIS program (Arabamer et al., 2020). Furthermore it reclassified them into five classes: 0–100, 100–200, and 200–300. 300-400 and >400 m, and >4000 m (Figure.4l).

4. Methodology

As, discussed earlier As discussed earlier, elevation, slope, aspect, curvature, slope length, relative relief, convergence index, lithology, thrust, fault, lineament, drainage density, drainage network, topographical wet index, rainfall, land use land cover (LULC), NDVI, road network along with landslide Inventory has been used for hazard mapping. All datasets were generated within a GIS environment at a pixel resolution of 5 × 5 m. The vector layers (i.e., landslide inventory, drainages, thrusts, and lithology/fault) corresponding to point, linear, and polygonal features were converted to raster format alongside other raster datasets such as elevation, slope, aspect and other parameters. All these raster datasets were converted to ASCII format using tools available in Erdas Imagine software. Thus, it can be read in SPSS for using Binary Logistic Regression (BLR) to predict landslide hazards. The database was further recoded in SPSS software for analysis purposes.

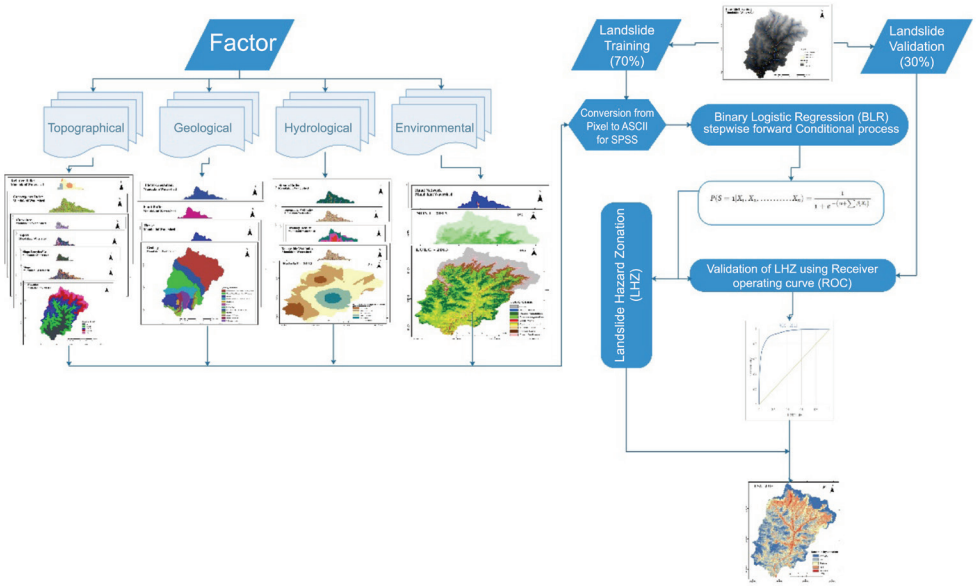

Figure 5 : Methodology Flow Diagram of Landslide Hazard Mapping over Study Area.

4.1 Binary Logistic Regression (BLR) Analysis

To determine the probability, BLR uses maximum likelihood estimation based on the logit variable, which is transformed from the dependent variable. The BLR framework is a type of generalized linear regression model where relevant independent variables influence the positive outcomes of dependent variables. For LHZ, a considerable benefit of the BLR model, in comparison to other multivariate statistical methods, is that it has probability values that range from 0 to 1 (Kleianbum, 1991; Kumar & Anbalagan, 2015). BLR can be expressed as –

$$P = \frac{1}{1+e^{-z}} \qquad \text{Eq. 4}$$

In this context, the estimated probability of landslide occurring is denoted by p, which is influenced by various causative factors. The probability is characterized by an

S-shaped curve, as described by Kleianbum (1991), and the linear combination denoted by z (as shown in Eq. 5) can range from $-\infty$ to $+\infty$. This unique aspect of the logistic function allows the logistic model to effectively assess the probability of slope failure risk for any specific grid. (Mathew et al., 2007a). z can be expressed as

$$Z = (\alpha + \sum_{i=1}^{n} \beta_i X_i) \qquad \text{Eq. 5}$$

Where,

α is the constant,

X_i is the independent variable, and

β_i is the corresponding coefficient

Thus, z is an index that combines the independent variables. By substituting Eq. 4.2 in 4.1, then it would be:

$$f(z) = \frac{1}{1+e^{-(\alpha+\sum \beta_i X_i)}} \qquad \text{Eq. 6}$$

Thus, the logistic model for slope failure can be expressed as:

$$P(S=1/X1,X2..... \ ... \ ... \ ... \ Xn = \frac{1}{1+e^{-(\alpha+\sum_{i=1}^{n} \beta i \, Xi)}} \qquad \text{Eq. 7}$$

where, P(S= 1|X1; X2; : . . . . . Xn) is the probability of a land unit–cell undergoing slope failure, given the presence of independent variables X1 to Xn. X1, X2……Xn

A constant (α) and the coefficients of the independent variables (βi) are among the regression parameters that are estimated by the model. Using a maximum likelihood approach, this estimation is based on the dependent variable's status inside the sample cells and the values of the independent variables (Mathew *et al.*, 2009). The value of

independent variables associated with causative factors is included in the database to estimate the BLR coefficients and the condition of the dependent variable, which indicates whether landslides are t present or absent of each pixel has been carefully assessed. It is assumed that the predictor variables are mutually independent. Every input parameter was acquired in raster format with a grid size of 5m x 5m. In the Mandakini watershed, 211233 (5 m×5 m) pixels were identified as landslide affected. Using a random sampling selection, 70% of landslide pixels, i.e.,147863, have been selected for the regression analysis, and the remaining 30% of landslide pixels (i.e., 63,370) have been retained for accuracy assessment. Similarly, an equal percentage (i.e.,70%) of the non-landslide pixels about 459,56890 (5 m×5 m) has been randomly selected from the study area, and the rest is used for accuracy assessment purposes.

4.2. Validation of the Model

The validation is crucial for landslide hazard mapping. The landslide hazard model will lack significance without validation. The assessment of model validity can be performed by juxtaposing the computed probability values for different cells with their actual states. This procedure is enabled through receiver operating characteristic (ROC) curve analysis (Zweig & Campbell, 1993). In this study, the ROC curve has been used (Kundu et al., 2013; Kumar & Anbalagan, 2015; Sun et al., 2018) to estimate the accuracy of the binary logistic regression model for landslide prediction, which is used as a quantitative measurement. The ROC curve illustrates the relationship between the probability of correctly identifying actual positive landslides and the probability of incorrectly identifying false positives, as the cut-off probability varies (Gorsevski et al., 2000). This curve effectively represents the trade-off between sensitivity (Sn) and specificity (Sp). Sensitivity, defined as the probability that a landslide cell is accurately classified, is represented on the y-axis of the ROC curve; conversely, one minus sensitivity reflects the false-negative rate. Specificity indicates the probability that a non-slide cell is correctly classified; similarly, one minus specificity corresponds to the false positive rate and is plotted along the x-axis of the curve (Hanley & McNeil, 1982). The area under the curve assesses the test's effectiveness in accurately

classifying pixels associated with landslide risk, both with and without it. The shape of the curve reflects the model's performance. A ROC plot that is positioned closer to the upper left corner indicates a higher overall accuracy of the test.

5. Results

5.1. Logistic Regression Coefficient

As discussed earlier, the forward stepwise BLR approach commenced with no variables out of 102 excluded in the first Step and terminated at the eighty-three steps, retaining 82 variables out of 102 variables. The BLR model attained a prediction accuracy of 89.6% (Table. 1), by classifying binary training data. The area under the curve assesses the test's effectiveness in accurately classifying pixels associated with landslide risk versus those without. The shape of the curve indicates the performance of the model. Table 2 presents the comprehensive model statistics from the regression analysis performed in this study utilizing SPSS. A critical component for the conventional analysis of the test is the model chi-square value, which provides a standard significance test for logistic regression, as referenced by Ayalew and Yamagishi (2005). In this study, the model chi-square value is notably high, suggesting that the independent factors significantly influence the occurrence of landslides. The elevated chi-square value indicates that landslides are less likely in the presence of the influencing parameters when compared to the complete regression model that includes all parameters. If the ROC plot approaches the upper left corner, it signifies higher overall accuracy for the test.

Table 1 : Classification Summary of the BLR Model at 83rd Step in 2013 (Post-disaster)

Observed					
			Landslide in 2013		Percentage Correct
			0 (No Landslide)	1 (Landslide)	
Step 83rd	Landslide in 2013	0 (No Landslide)	187364	23869	88.7
		1 (Landslide)	20278	190955	90.4
	Overall Percentage				89.6

Note: The cut value is .500

The Cox and Snell R^2 (1989) and Nagelkerke R^2 (1991) values always indicate how the model fits the data. According to Ayalew and Yamagishi (2005), an R^2 value of 1 indicates a perfect fit, while an R^2 value of 0 signifies no correlation with the data. Additionally, when the pseudo R^2 exceeds 0.2, it demonstrates relative goodness of fit (Clark and Hosking, 1986; Akgun, 2012). The statistical values computed for Cox and Snell R^2 (1989) and Nagelkerke R^2 (1991) in the 75th Step observed as 0.341 and 0.814 respectively, at 85th Step which indicates a good fit to the data.

Table 2 : The Overall Statistics of the BLR Model at 83rd Steps

Hosmer and Lemeshow Test			-2 Log likelihood	Cox & Snell R Square	Nagelkerke R Square
Chi-square	df	Sig.			
726.060	8	.000	943538.141	0.341	0.814

Note: Estimation terminated at iteration number 56 because parameter estimates changed by less than .001.

The BLR analysis has produced estimates for the constant and the coefficients of the independent variables. A positive logistic coefficient signifies that the independent variable enhances the likelihood of a landslide, while negative values imply an inverse association with landslide incidence (Vanwalleghem et al., 2008; Kundu. et al., 2013; Kumar & Anbalagan, 2015). The predictors retained in the final model and their estimated coefficients are given in Table. 3. The corresponding predicted probability value was represented by numbers falling between 0 and 1. The pixel value around 0 signifies a low likelihood of landslide, whereas the value near 1 denote a higher probability of landslide. The likelihood map of LHZ has been reclassified into five hazard zones viz. Very high hazard (VHH), High hazard (HH), Moderate hazard (MH), Low hazard (LH), and very low hazard (VLH) zone (Figure 7).

Table 3 : The Predictor Variables Retained in the BLR Model after 83rd Steps and their Coefficient

Category	Class	B	S.E.	Wald	df	Sig.	Exp(B)
Elevation	Elevation^2	.200	.014	191.446	1	.000	.819
	Elevation^3	.738	.020	1365.365	1	.000	.478
	Elevation^4	1.795	.025	5147.586	1	0.000	.166
	Elevation^5	-6.971	.448	241.686	1	.000	.001
Slope	Slope^1	-.391	.011	1163.212	1	.000	.676
	Slope^2	.119	.010	131.524	1	.000	.888
	Slope^3	.032	.009	11.937	1	.001	.969
Aspect	N	-.577	.022	704.284	1	.000	.562
	NE	-.040	.019	4.340	1	.037	.961
	E	.104	.019	31.339	1	.000	1.109
	SE	.048	.019	6.526	1	.011	1.049
	S	.184	.019	91.526	1	.000	.832
	SW	-.526	.020	697.800	1	.000	.591
	W	-.981	.023	1788.434	1	0.000	.375
	NW	-.453	.027	272.301	1	.000	.636
Curvature	Concave	-.054	.015	13.547	1	.000	.947
	Flat	.024	.007	11.247	1	.001	1.024
	Convex	-.089	.016	32.092	1	.000	.915

Category	Class	B	S.E.	Wald	df	Sig.	Exp(B)
Slope Length	SL^2	-.176	.014	165.609	1	.000	.839
	SL^4	.038	.018	4.407	1	.036	1.039
	SL^5	-.161	.033	23.806	1	.000	.851
Convergence Index	CI^1	.331	.014	587.783	1	.000	.718
	CI^4	-.163	.008	407.671	1	.000	.850
	CI^5	-.160	.017	89.305	1	.000	.852
Relative Relief	RR^1	.503	.023	480.374	1	.000	.604
	RR^3	.432	.015	844.264	1	.000	.649
	RR^4	-.883	.018	2407.819	1	0.000	.414
Lithology	Qp	2.409	.037	4268.100	1	0.000	11.124
	Ggsm	1.410	.034	1735.814	1	0.000	4.095
	PgMs	.400	.037	118.747	1	.000	1.492
	GgsCz	.804	.036	493.482	1	.000	2.236
	GgmsCz	.883	.035	651.925	1	.000	2.419
	Gr	1.311	.064	420.953	1	.000	3.710
	Me	-.170	.041	16.770	1	.000	.844
	Sq	.635	.064	98.184	1	.000	1.886
	Ps	-.564	.041	187.545	1	.000	.569
	Ph	.828	.056	215.400	1	.000	2.288

Category	Class	B	S.E.	Wald	df	Sig.	Exp(B)
Proximity to Fault	Fault[1]	.770	.018	1825.589	1	0.000	.463
	Fault[2]	.870	.021	1647.243	1	0.000	.419
	Fault[4]	-.061	.020	9.565	1	.002	.940
	Fault[5]	-.440	.021	453.755	1	.000	1.552
Proximity to Thrust	Thrust[2]	.059	.015	14.840	1	.000	.943
	Thrust[3]	.705	.014	2456.714	1	0.000	2.024
	Thrust[4]	.367	.016	516.093	1	.000	1.444
	Thrust[5]	-.539	.013	1715.239	1	0.000	1.714
Proximity to Lineament	PL[1]	.392	.060	43.297	1	.000	1.480
	PL[2]	.356	.055	42.347	1	.000	.701
	PL[4]	-.083	.031	7.312	1	.007	.921
	PL[5]	-1.280	.027	2166.872	1	0.000	3.596
Proximity to Stream Network	Stream[1]	.130	.008	257.120	1	.000	.878
	Stream[3]	-.809	.012	4631.871	1	0.000	.445
	Stream[4]	-1.084	.014	5892.538	1	0.000	.338
	Stream[5]	-1.872	.011	30603.150	1	0.000	.154
Drainage Density	DDensity[1]	-1.223	.020	3733.136	1	0.000	.294
	DDensity[2]	.032	.011	9.209	1	.002	1.033
	DDensity[3]	.037	.014	6.895	1	.009	.964
	DDensity[4]	-.232	.015	237.939	1	.000	.793

Category	Class	B	S.E.	Wald	df	Sig.	Exp(B)
Topographic Wet Index	TWI[1]	.099	.015	43.656	1	.000	1.104
	TWI[3]	-.053	.011	24.151	1	.000	.948
	TWI[4]	.055	.015	14.030	1	.000	1.056
	TWI[5]	-.020	.009	4.824	1	.028	.981
Relative Relief	RF2013[1]	-1.393	.022	4143.277	1	0.000	.248
	RF2013[2]	-.259	.011	530.505	1	.000	.772
	RF2013[4]	.437	.009	2377.798	1	0.000	1.548
	RF2013[5]	.883	.013	4941.515	1	0.000	2.417
Land Use Land Cover	Lulc2013[1]	2.066	.040	2611.439	1	0.000	7.894
	Lulc2013[2]	.615	.026	10008.199	1	0.000	13.668
	Lulc2013[3]	-1.717	.042	1676.225	1	0.000	.180
	Lulc2013[5]	1.511	.015	9775.722	1	0.000	4.530
	Lulc2013[6]	1.820	.014	16945.041	1	0.000	6.169
	Lulc2013[7]	2.830	.018	24762.329	1	0.000	16.937
	Lulc2013[8]	3.742	.015	59924.282	1	0.000	42.181
	Lulc2013[9]	3.892	.015	67963.527	1	0.000	48.987
Normalized Difference Vegetation Index	NDVI2013[1]	-.450	.016	765.200	1	.000	.638
	NDVI2013[2]	.072	.011	45.224	1	.000	.931
	NDVI2013[4]	.411	.018	550.464	1	.000	1.509
	NDVI2013[5]	-.161	.023	48.078	1	.000	1.174

Category	Class	B	S.E.	Wald	df	Sig.	Exp(B)
Distance from Road Network	DR^1	.109	.010	116.160	1	.000	1.115
	DR^3	-.653	.015	1930.250	1	0.000	.520
	DR^4	-.974	.018	2903.520	1	0.000	.377
	DR^5	-1.342	.012	13430.802	1	0.000	.261
	Constant	-7.430	.051	20926.029	1	0.000	.001

SE: Standard Error of estimate, Wald: Wald chi-square value, df: Degree of freedom, Sig: Significance, Exp(B): Exponentiated coefficient

5.2. Validation & Accuracy of the Model

LHZ was validated based on the ROC curve for the present study. The ROC curve analysis was done using the remaining 30% dataset of the presence of landslide pixels (i.e., 63,370) and absence of landslide pixels (i.e., 196,95,810). The area under the curve quantifies the test's effectiveness in accurately classifying pixels associated with landslide risk, both present and absent. The configuration of the curve reflects the model's performance. A curve that approaches the upper left corner of the ROC plot indicates a higher overall accuracy of the test. The area beneath the ROC curve reaches a maximum of 1 for flawless prediction, while a number approaching 0.5 indicates the model's inadequacy. The ROC curve for the present study is presented in Figures 6. The area under the curve was 0.914 (Table 4), indicating an accuracy of 91.4% for the model constructed by binary logistic regression. The standard error (0.006) and asymptotic signature value are found to be < 0.05, which indicates the validity of the ROC curve. The landslide hazard map generated by this model demonstrates effectiveness in predicting both known and previously unrecognized landslide occurrences.

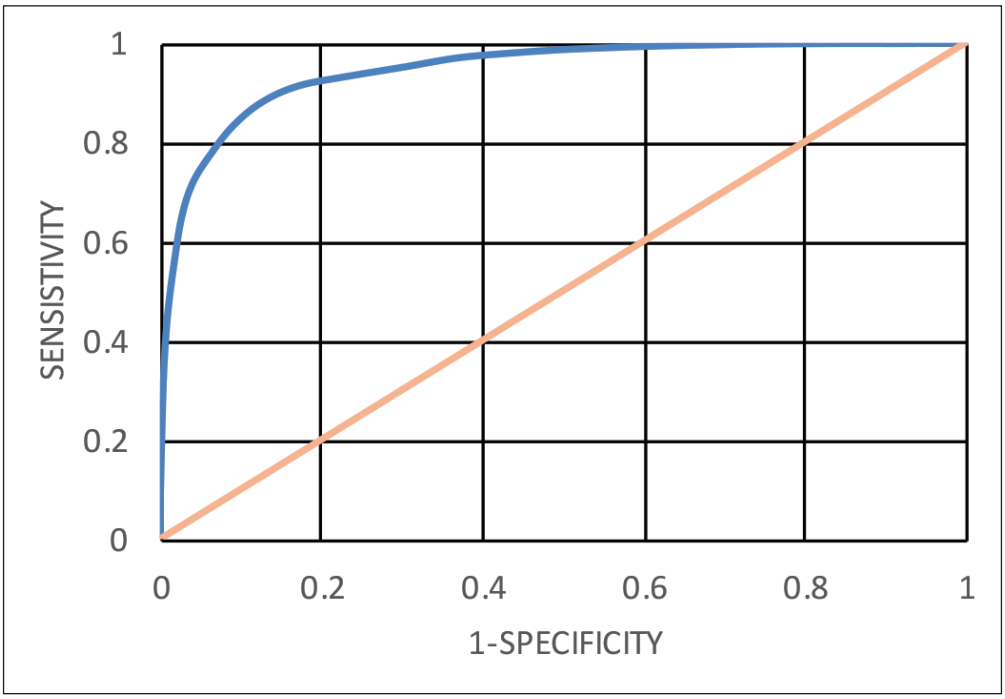

Figure 6 : ROC Curve of 2013 Showing Prediction Accuracy of LHZ Map.

Table 4 : Area under ROC Curve in 2013.

Area	Std. Error	Asymptotic Sig.[b]	Asymptotic 95% Confidence Interval	
			Lower Bound	Upper Bound
0.914	.006	0.000	0.905	0.926

Note: Larger values of the test result variable(s) indicate stronger evidence for a positive actual state.

a. Under the nonparametric assumption

b. Null hypothesis: true area = 0.5

6. Discussion

6.1. Analysis of BLR Result

Hazard Coefficients values (βi) in Table 4.7 suggest the significance of independent variables in determining the degree of landslide hazard in the study area. As mentioned earlier, positive and negative βi values influence the probability of a landslide. A positive βi value indicates that the corresponding classes contribute positively to the likelihood of landslide occurrence. In contrast, a negative βi value suggests a negative influence on landslide occurrence. In contrast, insignificant independent values do not result in βi values.

The binary logistic regression model selected 82 out of 102 initial independent variables in post-disaster Landslide Hazard Zonation (Table 4.7). The topographic factors Elevation class two, three, and four show positive βi value influence, whereas slope and slope length also have a positive βi value. Amongst the topographic attributes, the class two (15.71° - 25.03°0 and class three (25.03° - 33.47°) slope categories, while sloping length class four has positive βi value and class two and five resulted in a negative influence on slope failure. The Southeast, South, and East slope aspects show greater influence, creating slope instability than other aspect classes due to the higher solar insolation that these aspects receive in the Himalayan terrain. Flat curvature has also found positive βi value while concave and convex resulted in a negative impact on slope failure. Within the convergence Index class, one has a positive βi value for landslide conditioning. In the relative relief classes, a very high positive βi value is observed relief for the very low to medium comparative class (e.g., Class one and three). In contrast, negative βi is observed for the high relief class.

The next factor retained in the model is lithological units contributing towards slope instability. Within the lithological unit, higher βi found in Quartzite & Phyllite (Qp) and Granite (Gr) of the Garhwal Group flowed by Garnetiferous Gneiss Schist & Migmalite (Ggsm) of the Vaikrita group. In contrast, high βi observed in the Granitic Genesis Mica schist & Calc zone (GgmsCz) and Gneiss Garnetifarous Schist & Calc zone (GgsCz)

of Jutogh group flowed by phyllite (Ph) and Schistose Quartzite (Sq) of Garhwal and Vaikrita group respectively. Negative βi value found in Metabasies (Me) and Phyllite Slate (Ps) of the Garhwal group. The proximity of geological structures exhibits a relatively high estimated coefficient value, suggesting an increased likelihood of slope failure in regions with elevated values for this parameter. This phenomenon can be attributed to the diminished strength of the rock mass in areas characterized by a high density of geological discontinuities. Conversely, both the distance to confirmed thrusts and faults, as well as the distance to lineaments, demonstrate an inverse relationship; as the distance increases, their influence on slope destabilization correspondingly diminishes. Positive βi values are observed up to the distance of 1000 m in the case of the fault line and photo lineament, whereas in thrust, the Positive βi value is reflected for classes two, three, and from 500 m to 2000 m.

Within the study area, the Hydrology factor drainage density shows a high positive βi value in classes two and three, while high βi values are observed for the stream distance up to 100 m. In the topographic wet index class, one and four have positive βi values. Rainfall has found a strong relation with land sliding within the hydrological parameter. The High βi value has been found in classes three, four, and five of the rainfall zones. The fresh sediment, settlement, and barren land, under the land use land cover parameter, exhibits a significantly high value of Exp (βi), which indicates its susceptibility to slope failure. This phenomenon may be attributed to the absence of root-induced cohesion in the material, thereby increasing the likelihood of shallow landslides. Additionally, agricultural lands and water bodies also contribute to the potential for slope failure, as evidenced by the findings of this analysis. A very high βi value is also observed for distances up to 100 m of road, reflecting the contribution of fragile cut slopes left intact after the road construction.

6.2. Landslide Hazard Zonation

A landslide probability map has been created based on the statistical analysis and the output probabilities generated from the logistic regression model. The map has been categorized into various hazard classes utilizing natural break methods (NBM).

Worldwide, various literature shows that many methods are available to realize this necessity (Ayalew & Yamagishi, 2005; Lee, 2005).

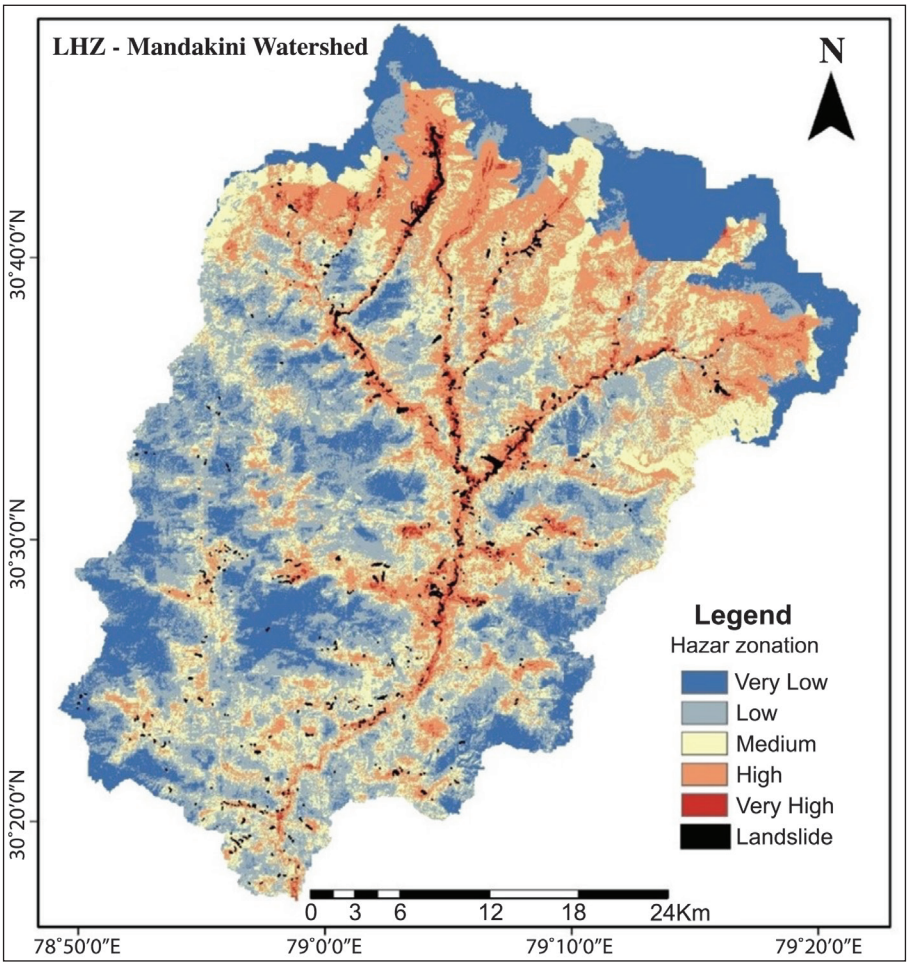

Figure 7 : Landslide Hazard Zonation Map of Mandakini Watershed in 2013

The natural breaks classification method segments the data to determine the best value arrangement in different classes. The NBM classification approach aims to minimise the average deviation from the mean class value while concurrently maximising the deviation from the means of other classes. Moreover, the NBM optimises

inter-class variance while minimising the intra-class variance (Arabamer et al., 2020). Therefore, five landslide hazard zones are identified for visual interpretation using the natural break methods, e.g., very low, low, medium, high, and very high zones. Figure 7 shows the landslide hazard zonation map with an overlay of observed landslides.

The landslide hazard zonation map shows that the very low hazard zone covers 18.89% of the entire study area, whereas low, medium, high, and very high hazard zones cover 31.95%, 27.05%, 19.57%, 2.54% of the total area, respectively. The landslide hazard zone map, developed through a logistic regression model, has been compared with the current landslide distribution layer. Figure 8 presents the percentage of the predicted hazard zones alongside the corresponding percentage of observed landslides within each zone. The 'very high hazard zone' encompasses about 2.54% of the overall area yet accounts for a significant 53.05% of landslide occurrences. Moreover, the landslide percentages in the 'high hazard zone' are significantly elevated at 37.80% in contrast to the area, which stands at merely 19.57%. The medium hazard zone encompasses 27.05% of the area and comprise merely 7.14% landslides. The low and very low hazard zones collectively comprise 50.84% of the territory with a landslide occurrence of 2.01% only.

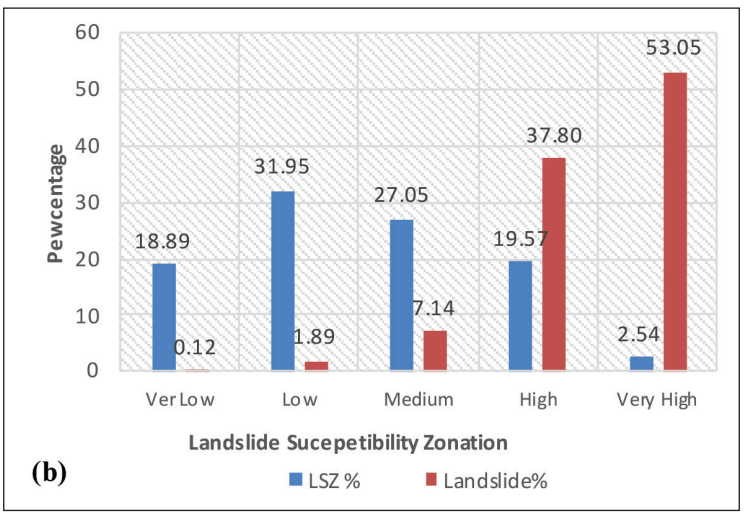

Figure 8 : Percentage Area of Predicted Landslide Hazard Zones and the Percentage of the Observed Landslides in each Zone of Mandakini Watershed.

7. Conclusion

The development of a landslide hazard map represents a crucial advancement in the pursuit of effective hazard management. In recent years, these maps have been generated using GIS-based qualitative and quantitative methodologies. This study is carried out in the Mandakini watershed of Garhwal Himalaya, which was vastly affected by the 2013 glacier lake outburst flood known as the Kedarnath Disaster. Many landslides were activated and newly emerged around Kedarnath, along the Mandakini River channel and NH 107 in 2013 nature fury. Binary logistic regression is a robust method for evaluating the likelihood of occurrence of a dichotomous dependent variable, such as a landslide, particularly in landslide-prone regions like the Himalayas. This method proves beneficial even when a significant number of the independent variables are categorical. The BLR model was terminated at the eighty-three steps, retaining 82 variables out of 102 independent variables. The BLR model achieved 89.6% prediction accuracy for Landslide Hazard Zonation over the study area by classifying binary training data. In the accuracy assessment through ROC, 91.4% accuracy was achieved using testing data. The findings demonstrate that the BLR model is both suitable and effective for the scale utilized in this study.

Analysis of Landslide hazard zonation revealed that the very low hazard zone covers 18.89% of the entire study area, whereas low, medium, high, and very high hazard zones cover 31.95%, 27.05%, 19.57%, 2.54% of the total area, respectively. Most of the high-hazard zones in Mandakini Valley fall along with human habitation and affect the connectivity network as well as the livelihood of the people. Therefore, it can be concluded that the 2013 disaster had a massive impact on the region's topography and resulted in increased vulnerability of the region. The increasing pattern of landslide events in very high and high-hazard zones needs to be monitored, and suitable management systems should be developed to reduce the further impact of landslide hazards.

References

1. Akgun, A. (2012). A comparison of landslide susceptibility maps produced by logistic regression, multi-criteria decision, and likelihood ratio methods: a case study at Izmir, Turkey. *Landslides*, 9(1): 93-106.
2. Arabameri, A., Saha, S., Roy, J., Chen, W., Blaschke, T., & Tien Bui, D. (2020). Landslide susceptibility evaluation and management using different machine learning methods in the Gallicash River Watershed, Iran. *Remote Sensing, 12*(3): 475.
3. Ayalew, L., & Yamagishi, H. (2005). The application of GIS-based logistic regression for landslide susceptibility mapping in the Kakuda-Yahiko Mountains, Central Japan. *Geomorphology, 65*(1-2): 15-31.
4. Bisht, S., Chaudhry, S., Sharma, S., & Soni, S. (2018). Assessment of flash flood vulnerability zonation through Geospatial technique in high altitude Himalayan watershed, Himachal Pradesh India. *Remote Sensing Applications: Society and Environment, 12*: 35-47.
5. Carrara, A., Cardinali, M., Guzzetti, F., & Reichenbach, P. (1995). GIS technology in mapping landslide hazard. In *Geographical information systems in assessing natural hazards* (pp. 135-175). Springer, Dordrecht.
6. Chahal, P., Rana, N., Bisht, P., Bagri, D. S., Wasson, R. J., & Sundriyal, Y. (2017). Identification of landslide-prone zones in the geomorphically and climatically sensitive Mandakini valley, (central Himalaya), for disaster governance using the Weights of Evidence method. *Geomorphology, 284*: 41-52.
7. Choubey, V. M., Bist, K. S., Saini, N. K., & Ramola, R. C. (1999). Relation between soil-gas radon variation and different lithotectonic units, Garhwal Himalaya, India. Applied Radiation and Isotopes, 51(5): 587-592.
8. Clark, W.A. and Hosking, P.L., 1986. Statistical Methods for Geographers.*John Wiley and Sons*, New York. 518 pp.
9. Cox, D.R. and Snell, E.J. (1989). The analysis of binary data. (2nd Ed.) Chapman and Hall, London, 236p.
10. Das S. & Saha A. K., (2020) Identification of Landslide-prone Zones of Mandakini Valley (Central Himalaya) Post-Kedarnath Tragedy (2013) – Annals of the National Association of Geographers, India^, 40(2):304-329 [ISSN: 0970-972X (Print)] [https://doi.org/10.32381/ATNAGI.2020.40.02.8]
11. Dahal, R. K., Hasegawa, S., Nonomura, A., Yamanaka, M., Masuda, T., & Nishino, K. (2008b). GIS-based weights-of-evidence modelling of rainfall-induced landslides in small catchments for landslide susceptibility mapping. *Environmental Geology, 54*(2): 311-324.
12. Dietrich, W. E., Reiss, R., Hsu, M. L., & Montgomery, D. R. (1995). A process-based model for colluvial soil depth and shallow landsliding using digital elevation data. *Hydrological processes, 9*(3-4): 383-400.
13. Dubey, C. S., Shukla, D. P., Ningreichon, A. S., & Usham, A. L. (2013). Orographic control of the Kedarnath disaster. *Current Science, 105*(11): 1474-1476.
14. Ercanoglu, M., & Gokceoglu, C. (2004). Use of fuzzy relations to produce landslide susceptibility map of a landslide prone area (West Black Sea Region, Turkey). *Engineering Geology, 75*(3-4): 229-250.
15. Fell, R., Hungr, O., Leroueil, S., & Riemer, W. (2000, November). Keynote lecture-geotechnical engineering of the stability of natural slopes, and cuts and fills in soil. In *ISRM International Symposium*. International Society for Rock Mechanics and Rock Engineering.
16. Furlani, S., & Ninfo, A. (2015). Is the present the key to the future?. *Earth-Science Reviews*, 142: 38-46.
17. Glade, T., & Crozier, M. (1996). Towards a national landslide information base for New Zealand. *New Zealand Geographer*, 52(1): 29-40.
18. Gorsevski, P. V., Gessler, P., & Foltz, R. B. (2000a). Spatial prediction of landslide hazard using discriminant analysis and GIS. In In: *GIS in the Rockies 2000 Conference and Workshop: applications for the 21st Century, Denver, Colorado, September 25-27, 2000.*
19. Goovaerts, P. (2000). Geostatistical approaches for incorporating elevation into the spatial interpolation of rainfall. *Journal of hydrology, 228*(1-2): 113-129.
20. Guzzetti, F., Carrara, A., Cardinali, M., & Reichenbach, P. (1999). Landslide hazard evaluation: a review of current techniques and their application in a multi-scale study, Central Italy. *Geomorphology*, 31(1-4): 181-216.
21. Guzzetti, F., Mondini, A. C., Cardinali, M., Fiorucci, F., Santangelo, M., & Chang, K. T. (2012). Landslide inventory maps: New tools for an old problem. *Earth-Science Reviews*, 112(1-2): 42-66.
22. Hadmoko, D. S., Lavigne, F., Sartohadi, J., & Hadi, P. (2010). Landslide hazard and risk assessment and their application in risk management and landuse planning in eastern flank of Menoreh Mountains, Yogyakarta Province, Indonesia. *Natural Hazards, 54*(3): 623-642.
23. Hanley, J. A., & McNeil, B. J. (1982). The meaning and use of the area under a receiver operating characteristic (ROC) curve. *Radiology, 143*(1): 29-36.
24. Hamza, T., & Raghuvanshi, T. K. (2017). GIS based landslide hazard evaluation and zonation–A case from Jeldu District, Central Ethiopia. *Journal of King Saud University-Science, 29*(2): 151-165.
25. Horton, R. E. (1945). Erosional development of streams and their drainage basins; hydrophysical approach to quantitative morphology. *Geological society of America bulletin, 56*(3): 275-370.
26. Huabin, W., Gangjun, L., Weiya, X., & Gonghui, W. (2005). GIS-based landslide hazard assessment: an overview. *Progress in Physical geography, 29*(4): 548-567.

27. Kayastha, P., Dhital, M. R., & De Smedt, F. (2013). Application of the analytical hierarchy process (AHP) for landslide susceptibility mapping: A case study from the Tinau watershed, west Nepal. *Computers & Geosciences, 52*: 398-408.
28. Khanduri, S., Sajwan, K. S., Rawat, A., Dhyani, C., & Kapoor, S. (2018). Disaster in Rudraprayag District of Uttarakhand Himalaya: a special emphasis on geomorphic changes and slope instability. *J Geogr Nat Disast, 8*(218): 2167-0587.
29. Kleinbaum, D.G., (1991). Logistic Regression: a Self-learning Text. Springer, Berlin Heidelberg New York.
30. Kumar, R., & Anbalagan, R. (2015). Landslide susceptibility zonation of Tehri reservoir rim region using binary logistic regression model. *Current Science*, 1662-1672.
31. Kumar, R., & Anbalagan, R. (2019). Landslide susceptibility mapping of the Tehri reservoir rim area using the weights of evidence method. *Journal of Earth System Science*, 128(6): 1-18.
32. Kundu, S., Saha, A. K., Sharma, D. C., & Pant, C. C. (2013). Remote sensing and GIS based landslide susceptibility assessment using binary logistic regression model: a case study in the Ganeshganga Watershed, Himalayas. *Journal of the Indian Society of Remote Sensing*, 41(3): 697-709.
33. Lee, S., & Min, K. (2001). Statistical analysis of landslide susceptibility at Yongin, Korea. *Environmental geology, 40*(9): 1095-1113.
34. Lee, S., Ryu, J. H., Won, J. S., & Park, H. J. (2004). Determination and application of the weights for landslide susceptibility mapping using an artificial neural network. *Engineering Geology, 71*(3-4): 289-302.
35. Lee, S. (2005). Application of logistic regression model and its validation for landslide susceptibility mapping using GIS and remote sensing data. *International Journal of remote sensing, 26*(7): 1477-1491.
36. Lee, S., Hwang, J., & Park, I. (2013). Application of data-driven evidential belief functions to landslide susceptibility mapping in Jinbu, Korea. *Catena*, 100: 15-30.
37. Li, J. X., Wang, C. M., & Wang, G. C. (2013). Landslide risk assessment based on combination weighting-unascertained measure theory. *Rock and Soil Mechanics, 34*(2): 468-474.
38. Mathew, J., Jha, V. K., & Rawat, G. S. (2007a). Application of binary logistic regression analysis and its validation for landslide susceptibility mapping in part of Garhwal Himalaya, India. *International Journal of Remote Sensing, 28*(10): 2257-2275.
39. Mathew, J., Jha, V. K., & Rawat, G. S. (2009). Landslide susceptibility zonation mapping and its validation in part of Garhwal Lesser Himalaya, India, using binary logistic regression analysis and receiver operating characteristic curve method. *Landslides*, 6(1): 17-26.
40. Mondini, A. C., Guzzetti, F., Reichenbach, P., Rossi, M., Cardinali, M., & Ardizzone, F. (2011). Semi-automatic recognition and mapping of rainfall induced shallow landslides using optical satellite images. *Remote Sensing of Environment, 115*(7): 1743-1757.
41. Moore, I. D., Grayson, R. B., & Ladson, A. R. (1991). Digital terrain modelling: a review of hydrological, geomorphological, and biological applications. *Hydrological processes, 5*(1): 3-30.
42. Nagelkerke, N. J. (1991). A note on a general definition of the coefficient of determination. *Biometrika*, 78(3): 691-692.
43. Naithani, A. K., Rawat, G. S., & Nawani, P. C. (2011). Investigation of landslide events on 12th July 2007 due to cloudburst in Chamoli district, Uttarakhand, India. *International Journal of Earth Sciences and Engineering, 4*(5): 777-786.
44. Pandey, A., Dabral, P. P., Chowdary, V. M., & Yadav, N. K. (2008). Landslide hazard zonation using remote sensing and GIS: a case study of Dikrong river basin, Arunachal Pradesh, India. *Environmental geology*, 54(7): 1517-1529.
45. Pardeshi, S. D., Autade, S. E., & Pardeshi, S. S. (2013). Landslide hazard assessment: recent trends and techniques. *SpringerPlus, 2*(1): 1-11.
46. Pourghasemi, H. R., Pradhan, B., & Gokceoglu, C. (2012a). Application of fuzzy logic and analytical hierarchy process (AHP) to landslide susceptibility mapping at Haraz watershed, Iran. *Natural hazards, 63*(2): 965-996.
47. Pourghasemi, H. R., Pradhan, B., Gokceoglu, C., Mohammadi, M., & Moradi, H. R. (2012b). Application of weights-of-evidence and certainty factor models and their comparison in landslide susceptibility mapping at Haraz watershed, Iran. *Arabian Journal of Geosciences, 6*(7): 2351-2365.
48. Pradhan, A. M. S., & Kim, Y. T. (2014). Relative effect method of landslide susceptibility zonation in weathered granite soil: a case study in Deokjeok-ri Creek, South Korea. *Natural hazards*, 72(2): 1189-1217.
49. Pradhan, B., & Lee, S. (2010). Landslide susceptibility assessment and factor effect analysis: backpropagation artificial neural networks and their comparison with frequency ratio and bivariate logistic regression modelling. *Environmental Modelling & Software, 25*(6): 747-759.
50. Qiu, H., Regmi, A. D., Cui, P., Hu, S., Wang, Y., & He, Y. (2017). Slope aspect effects of loess slides and its spatial differentiation in different geomorphologic types. *Arabian Journal of Geosciences, 10*(15): 1-12.
51. Reichenbach, P., Mondini, A. C., & Rossi, M. (2014). The influence of land use change on landslide susceptibility zonation: the Briga catchment test site (Messina, Italy). *Environmental management, 54*(6): 1372-1384.
52. Rozos, D., Bathrellos, G. D., & Skillodimou, H. D. (2011). Comparison of the implementation of rock engineering

system and analytic hierarchy process methods, upon landslide susceptibility mapping, using GIS: a case study from the Eastern Achaia County of Peloponnesus, Greece. *Environmental Earth Sciences, 63*(1): 49-63.
53. Saadatkhah, N., Kassim, A., & Lee, L. M. (2015). Susceptibility assessment of shallow landslides in Hulu Kelang area, Kuala Lumpur, Malaysia using analytical hierarchy process and frequency ratio. *Geotechnical and Geological Engineering, 33*(1): 43-57.
54. Saha, A. K., Gupta, R. P., & Arora, M. K. (2002). GIS-based landslide hazard zonation in the Bhagirathi (Ganga) valley, Himalayas. *International journal of remote sensing, 23*(2): 357-369.
55. Saha, A. K., Gupta, R. P., Sarkar, I., Arora, M. K., & Csaplovics, E. (2005). An approach for GIS-based statistical landslide susceptibility zonation—with a case study in the Himalayas. *Landslides, 2*(1): 61-69.
56. Sahana, M., & Sajjad, H. (2017). Evaluating effectiveness of frequency ratio, fuzzy logic and logistic regression models in assessing landslide susceptibility: a case from Rudraprayag district, India. *Journal of Mountain Science, 14*(11): 2150-2167.
57. Sati, S. P., & Gahalaut, V. K. (2013). The fury of the floods in the north-west Himalayan region: the Kedarnath tragedy. *Geomatics, Natural Hazards and Risk, 4*(3): 193-201.
58. Sharma, S., & Mahajan, A. K. (2018). Comparative evaluation of GIS-based landslide susceptibility mapping using statistical and heuristic approach for Dharamshala region of Kangra Valley, India. *Geoenvironmental Disasters, 5*(1): 1-16.
59. Sun, X., Chen, J., Bao, Y., Han, X., Zhan, J., & Peng, W. (2018). Landslide susceptibility mapping using logistic regression analysis along the Jinsha river and its tributaries close to Derong and Deqin County, southwestern China. ISPRS *International Journal of Geo-Information, 7*(11): 438.
60. Sundriyal, Y. P., Shukla, A. D., Rana, N., Jayangondaperumal, R., Srivastava, P., Chamyal, L. S., & Juyal, N. (2015). Terrain response to the extreme rainfall event of June 2013: Evidence from the Alaknanda and Mandakini River Valleys, Garhwal Himalaya, India. *Episodes, 38*(3): 179-188.
61. Thanh, L. N., & De Smedt, F. (2012). Application of an analytical hierarchical process approach for landslide susceptibility mapping in A Luoi district, Thua Thien Hue Province, Vietnam. *Environmental Earth Sciences, 66*(7): 1739-1752.
62. Tien Bui, D., Pradhan, B., Lofman, O., & Revhaug, I. (2012). Landslide susceptibility assessment in vietnam using support vector machines, decision tree, and Naive Bayes Models. *Mathematical problems in Engineering, 2012.*
63. Valdiya, K. S. (1980). *Geology of kumaun lesser Himalaya*. Wadia Institute of Himalayan Geology.
64. Valdiya, K. S. (2014). Damming rivers in the tectonically resurgent Uttarakhand Himalaya. *Current Science:* 1658-1668.
65. van Beek, L. P. H. (2002). *Assessment of the influence of changes in land use and climate on landslide activity in a Mediterranean environment* (Doctoral dissertation).
66. van der Knijff, J. M., Jones, R. J. A., & Montanarella, L. (2000). Soil erosion risk: assessment in Europe.
67. Vanwalleghem, T., Van Den Eeckhaut, M., Poesen, J., Govers, G., & Deckers, J. (2008). Spatial analysis of factors controlling the presence of closed depressions and gullies under forest: Application of rare event logistic regression. *Geomorphology, 95*(3-4): 504-517.
68. Van Westen, C. J., Rengers, N., & Soeters, R. (2003). Use of geomorphological information in indirect landslide susceptibility assessment. *Natural hazards, 30*(3): 399-419.
69. van Asselen, S., & Seijmonsbergen, A. C. (2006). Expert-driven semi-automated geomorphological mapping for a mountainous area using a laser DTM. Geomorphology, 78(3-4): 309-320.
70. Van Westen, C. J., Van Asch, T. W., & Soeters, R. (2006). Landslide hazard and risk zonation—why is it still so difficult?. *Bulletin of Engineering geology and the Environment, 65*(2): 167-184.
71. Van Westen, C. J., Castellanos, E., & Kuriakose, S. L. (2008). Spatial data for landslide susceptibility, hazard, and vulnerability assessment: An overview. *Engineering geology, 102*(3-4): 112-131.
72. Wang, Q., Li, W., Chen, W., & Bai, H. (2015). GIS-based assessment of landslide susceptibility using certainty factor and index of entropy models for the Qianyang County of Baoji city, China. *Journal of Earth System Science, 124*(7): 1399-1415.
73. Yalcin, A., & Bulut, F. (2007). Landslide susceptibility mapping using GIS and digital photogrammetric techniques: a case study from Ardesen (NE-Turkey). *Natural Hazards, 41*(1): 201-226.
74. Yang, X., & Chen, L. (2010). Using multi-temporal remote sensor imagery to detect earthquake-triggered landslides. *International Journal of Applied Earth Observation and Geoinformation, 12*(6): 487-495.
75. Zhang, F., Chen, W., Liu, G., Liang, S., Kang, C., & He, F. (2012). Relationships between landslide types and topographic attributes in a loess catchment, China. *Journal of Mountain Science, 9*(6): 742-751.
76. Zweig, M. H., & Campbell, G. (1993). Receiver-operating characteristic (ROC) plots: a fundamental evaluation tool in clinical medicine. *Clinical chemistry, 39*(4): 561-577.